Intermetallics 127 (2020) 106984

Contents lists available at ScienceDirect

Intermetallics

journal homepage: http://www.elsevier.com/locate/intermet

Alloying effect on solidification behaviour and grain refinement in Ti45Al2Nb2Ta0.8B and Ti45Al2Nb2Hf0.8B

Jing Li [a,*], Spencer Jeffs [a], Mark Whittaker [a], Nigel Martin [b]

[a] Institute of Structural Materials, Swansea University, Fabian Way, Swansea, SA1 8EN, UK
[b] Rolls-Royce Plc, Derby, DE24 8BJ, UK

ARTICLE INFO

Keywords:
Titanium aluminide
TiAl
Solidification
Microstructure
Grain refinement
Boron

ABSTRACT

The solidification process of Ti45Al2Nb2Ta0.8B (B4522Ta) and Ti45Al2Nb2Hf0.8B (B4522Hf) Bridgman samples were studied through directional solidification. Boron addition at 0.8 at. % was found to have changed the orientation relationship of peritectic α with β dendrites. The peritectic alpha is randomly oriented in both B4522Ta and B4522Hf, it was likely to be inoculated by boride precipitates at the β/liquid interfaces during peritectic transformation. The alloying effect of Ta and Hf on the peritectic reaction was similar. Borides precipitated earlier in Ta-containing alloy than that in Hf-containing alloy during solidification.

1. Introduction

Introducing boron into titanium aluminide to refine microstructures stretches back to the development of Ti4522XD almost thirty years ago, with boron continuing to be a grain refiner in the latest wrought beta-solidifying TNM alloys [1]. The refined grain size can be as small as 20–150 μm depending on the cooling conditions during solidification. Investment casting is probably the most cost-effective technique to date for producing complicated low pressure turbine (LPT) blades due to its ability for large scale production and near net-shape forming. Ti45Al2Mn2Nb1B is an alloy most suitable for near net-shape LPT blade castings owing not only to its excellent castability but also its fine microstructures in as-cast condition, which makes the post-casting heat treatment simple [2,3]. However, the temperature capability of Ti45Al2Mn2Nb1B limits the range of application in LP turbines. Therefore, more novel systems have resulted in the inclusion of more or new refractory elements, such as Nb, Hf, Ta, Mo and W, which may improve oxidation/corrosion resistance and creep resistance thus improving alloys' overall temperature capability. Ti45Al2Mn2Nb1B solidify via the peritectic reaction (L + β → α) according to the phase diagram with the assumption that the minor alloying additions do not cause significant deviation [4]. The understanding of the grain refinement mechanism in TiAl–B alloys with peritectic reaction solidification paths has been far from satisfactory despite some already proposed universal grain refinement mechanisms [2,5–9]. Previous studies reported by Li et al. [10] has investigated the Hf and Ta partitioning behaviour in boride. Hf promotes formation of thin curvy boride flakes, whereas Ta promotes formation of thick straight boride ribbons, regardless of the alloy composition. Liu et al. [11] has reported that TiB particles are enriched with Nb and Ta, but depleted with Mn. The directional solidification technique proven to be a powerful and effective method to study the solidification process in TiAl alloys [12]. This paper presents the results from a study on the solidification behaviour of variants of Ti4522–1B, which are Ti–45Al–2Nb–2Ta-0.8B and Ti–45Al–2Nb-2Hf-0.8B, with emphasis on the peritectic reaction, boride precipitation temperature and to extend the knowledge spectrum of understanding the grain refinement mechanism in boron containing TiAl alloys with Ta and Hf additions.

2. Experimental

The Bridgman technique has been proved an effective method to study the solidification process because the different microstructures existing at different temperatures can be traced back through known phase transformations. Ti45Al2Nb2Ta0.8B and Ti45Al2Nb2Hf0.8B Bridgman samples, referred to as B4522Ta and B4522Hf respectively, were prepared from a plasma arc melted 1 kg hemispherical button ingot. The buttons were melted four times with ~90° turning each time before the next melting to improve homogeneity. Cylinders 8 mm in diameter were taken from the buttons as the feedstock for preparing Bridgman specimens. The samples were produced in a vertical Bridgman-Stockbarger furnace in ACCESS Materials and Process in

* Corresponding author.
E-mail address: jing.li@swansea.ac.uk (J. Li).

https://doi.org/10.1016/j.intermet.2020.106984
Received 20 July 2020; Received in revised form 10 September 2020; Accepted 25 September 2020

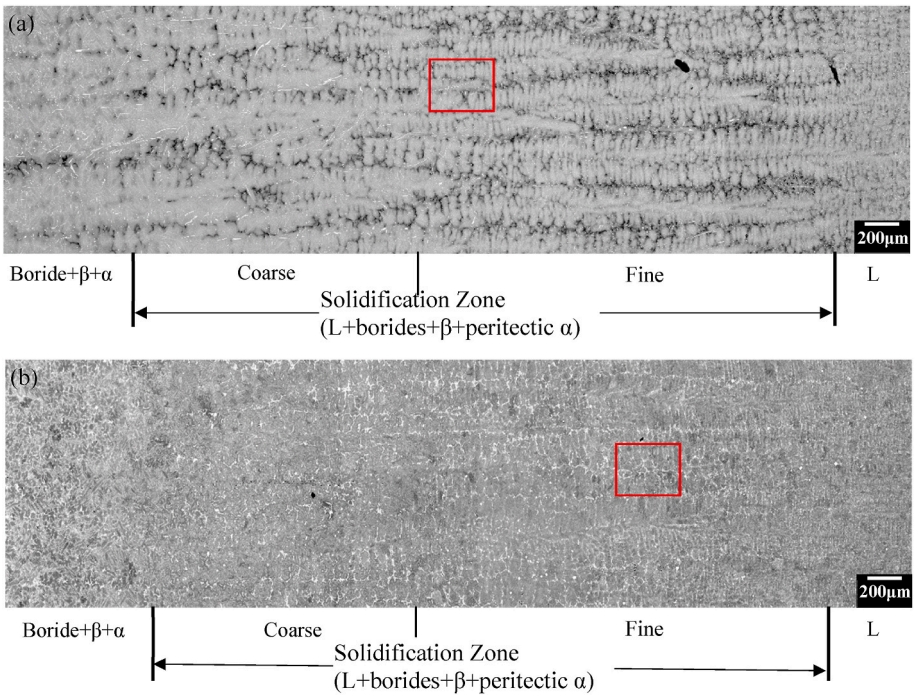

Fig. 1. BSE image montages showing the microstructures of the solidification zone in (a) B4522Ta and (b) B4522Hf Bridgman specimens. The withdrawal direction is to the left.

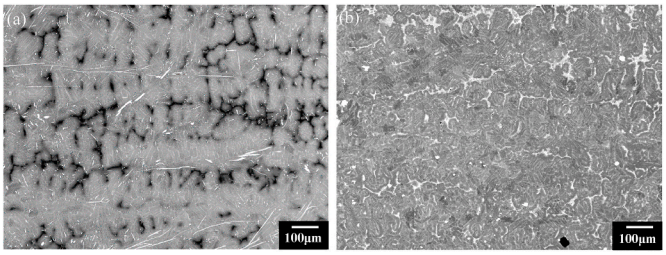

Fig. 2. BSE images of enlarged coarse dendritic zone in the solidification zone of (a) B4522Ta and (b) B4522Hf Bridgman specimens.

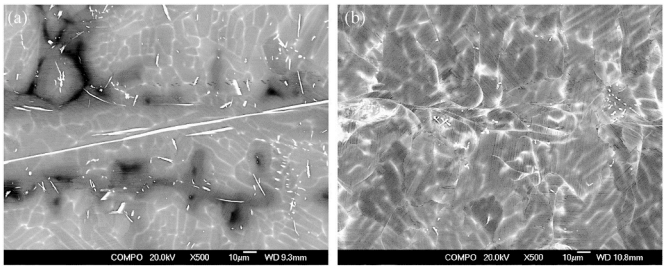

Fig. 3. BSE images of enlarged microstructures quenched from solidification zone in (a) B4522Ta and (b) B4522Hf. Red boxes highlighted in Fig. 1 show where these BSE images were taken from the solidification zone.

Germany. This method involves remelting feedstock which was contained in densely sintered yttria crucible tubes prior to withdrawal at a constant velocity of 8.33×10^{-5} m·s^{-1} through a constant temperature gradient in liquid at the solid-liquid interface of G_L 2×10^4 °C·m^{-1}. The furnace operates under 1000 mbar Argon, with oxygen content at ~500 wtppm. Solidification process was frozen by liquid metal quenching with a cooling rate of about 100 °C·s^{-1} and preserving the mushy zone for subsequent analysis. Details of the setup of the furnace and other parameters can be found in Ref. [13]. The Bridgman specimens were sliced longitudinally and polished using common preparation methods and areas of interest were analysed using scanning electron microscopy (SEM) and electron backscattered diffraction (EBSD).

3. Results and discussion

3.1. General description of microstructures

The overview of the microstructures along the longitudinal section of the unidirectional solidified B4522Ta and B4522Hf are shown in Fig. 1. The overall microstructure can be classified into three zones which are quenched liquid, the solidification zone (mushy zone), and the complete solid zone. The solidification zone features dendrites in different sizes, which can be further divided into the coarse dendritic zone and fine dendritic zone. Micrographs were taken in the back-scatter electron (BSE) mode and thus the contrast was mainly compositional. Fig. 2 shows the BSE images of enlarged coarse dendritic zone in the solidification zone. The white particles are yttrium which is melt contamination from crucible walls. Two significant differences can be seen by comparing the solidification zones of the two alloys. The first is that the dendrites in B4522Hf are much finer than those in B4522Ta. The second is that the contrast between β dendrite and the interdendritic region in B4522Ta is much stronger than that in B4522Hf. These differences can be attributed to the different alloying additions since the two Bridgman specimens were prepared under the same conditions and same boron concentration. The interdendritic region in B4522Ta shows dark contrast, exhibits microsegregation that is rich in Al and lean in Nb and Ta. However, the interdendritic region in B4522Hf shows bright contrast and exhibits microsegregation that is lean in Al and rich in Nb and Hf.

Detailed microstructures of the solidification zone of B4522Ta and B4522Hf are shown in Fig. 3 (a) and Fig. 3 (b), respectively. Both micrographs were taken from the middle of the solidification zone. Bright ridges can be observed within some β dendrites, which is indicative of the β → α phase transformation. Their existence implies that those parts of dendrites were β phase before quenching. During transformation, the β stabilizing elements, e.g Ta and Nb, were expelled from the newly

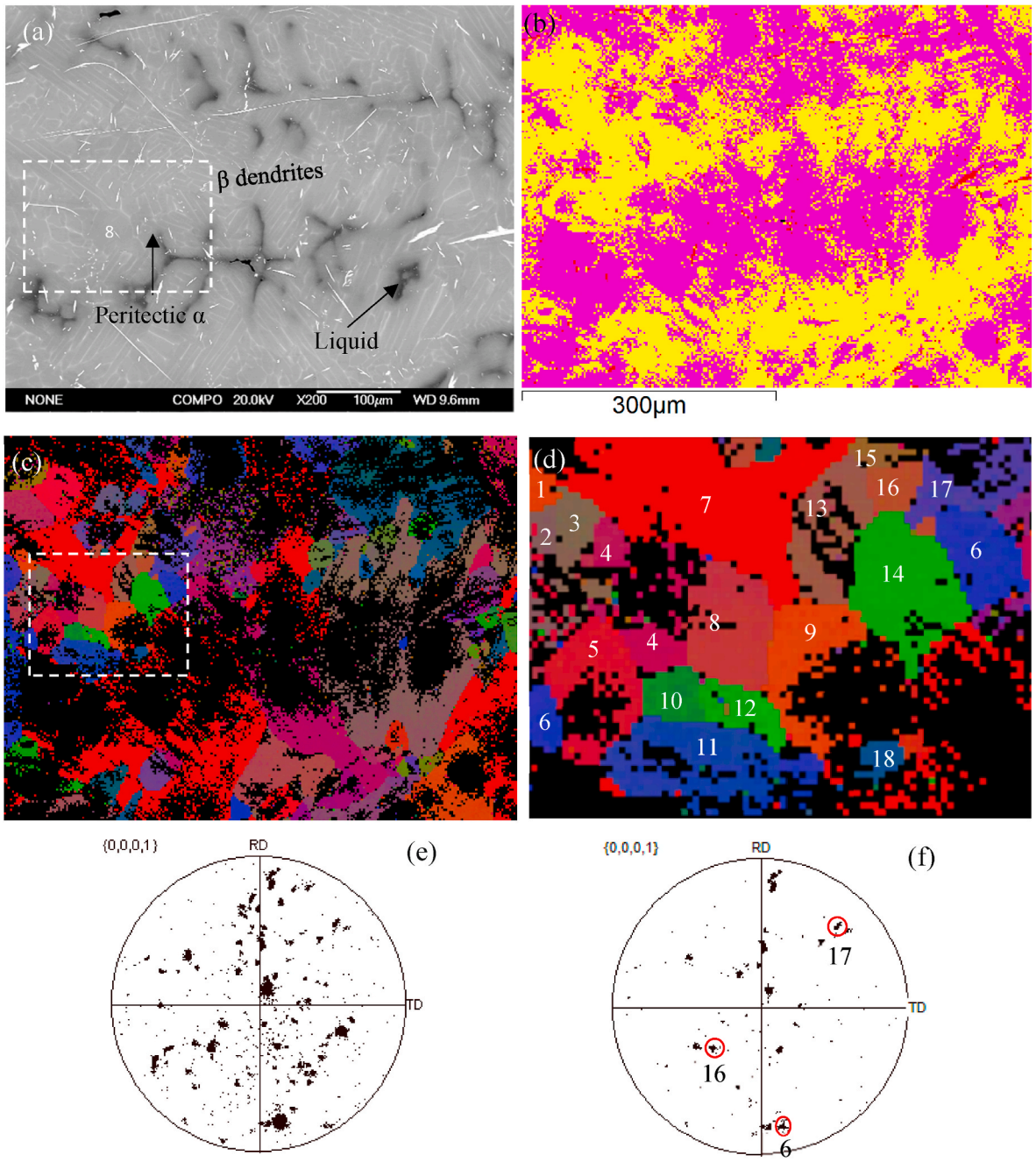

Fig. 4. Coarse dendritic region in B4522Ta Bridgman sample showing (a) microstructure with original phase before quenching indicated, (b) phase map in which , and represent α2, γ and TiB phases, respectively, (c) α2 phase normal direction orientation map, (d) enlarged α2 normal orientation map, (e) α (0001) pole figures of the whole area, (f) α (0001) pole figures of the selected grains.

formed α to the remaining β. These areas are enriched with β stabilizing elements even after they eventually transformed into α entirely, which thus gives rise to bright contrast in BSE images. No such micro-segregation can be observed in the peritectic α grains, which have higher Al and B content than β dendrites but lower Al than the interdendritic liquid.

3.2. Titanium boride

Titanium boride precipitates are evident in the solidification zone. Boride precipitates in B4522Ta are coarse, long and embedded within the β dendrites with some parallel to the stems of the dendrites. It indicates that those borides should have grown in conjunction with the β dendrites or were slightly later than the leading β phase during solidification. The strong contrast of TiB precipitates under BSE mode is because Ta strongly segregates into boride, forming (Ti, Ta)B. Conversely, in B4522Hf, fine curvy borides are found in the interdendritic areas at an early stage of solidification, most of them are formed during quenching, which indicates that the boride formation occurred well after the β dendrites were formed, probably at a stage when the β dendrite growth was almost to its end. This observation suggests that Ta and Hf affect boride precipitation temperature (relative temperature in L + S region) differently. Borides in the Ta-containing alloy precipitate earlier than in the Hf-containing alloy, therefore, borides have enough time and space to grow freely in all directions even though the fastest growing directions are still favoured. It suggests that Ta and Hf shift the

Table 1
Angle between c-axes of the selected α_2 grains in coarse dendritic area in B4522Ta.

	α17	α16
α16	120.5	
α6	122.1	58.9

phase boundaries to extend the high-temperature β phase to higher Al concentrations, although Hf shifts the phase boundary to a lesser extent than Ta [14–16]. It is inferred from these observations that the onset of borides are not only affected by the cooling rate during solidification but also the alloying element species.

The crystal structure of coarse long boride and fine curvy boride were identified using TEM as having a B27 structure (orthorhombic with a = 0.611 nm, b = 0.305 nm and c = 0.456 nm) and a B_f structure (orthorhombic with a = 0.323 nm, b = 0.856 nm and c = 0.305 nm), respectively. Orientation relationships were observed between borides and α_2 grains, which are:

$$< 11\bar{2}0>_{\alpha 2} // [010]_{B27}, (0001)_{\alpha 2}//(001)_{B27} \quad (1)$$

$$< 11\bar{2}0 >_{\alpha 2} // [001]_{Bf}, (0001)_{\alpha 2}// (110)_{Bf} \quad (2)$$

3.3. Peritectic transformation

According to the Ti–Al binary phase diagram, in alloys with Al concentration of 44.8–49.4 at. %, there is a peritectic reaction, L + β → α. Both B4522Ta and B4522Hf fall into this composition range, assuming that low alloying elements will not cause a large shift of phase

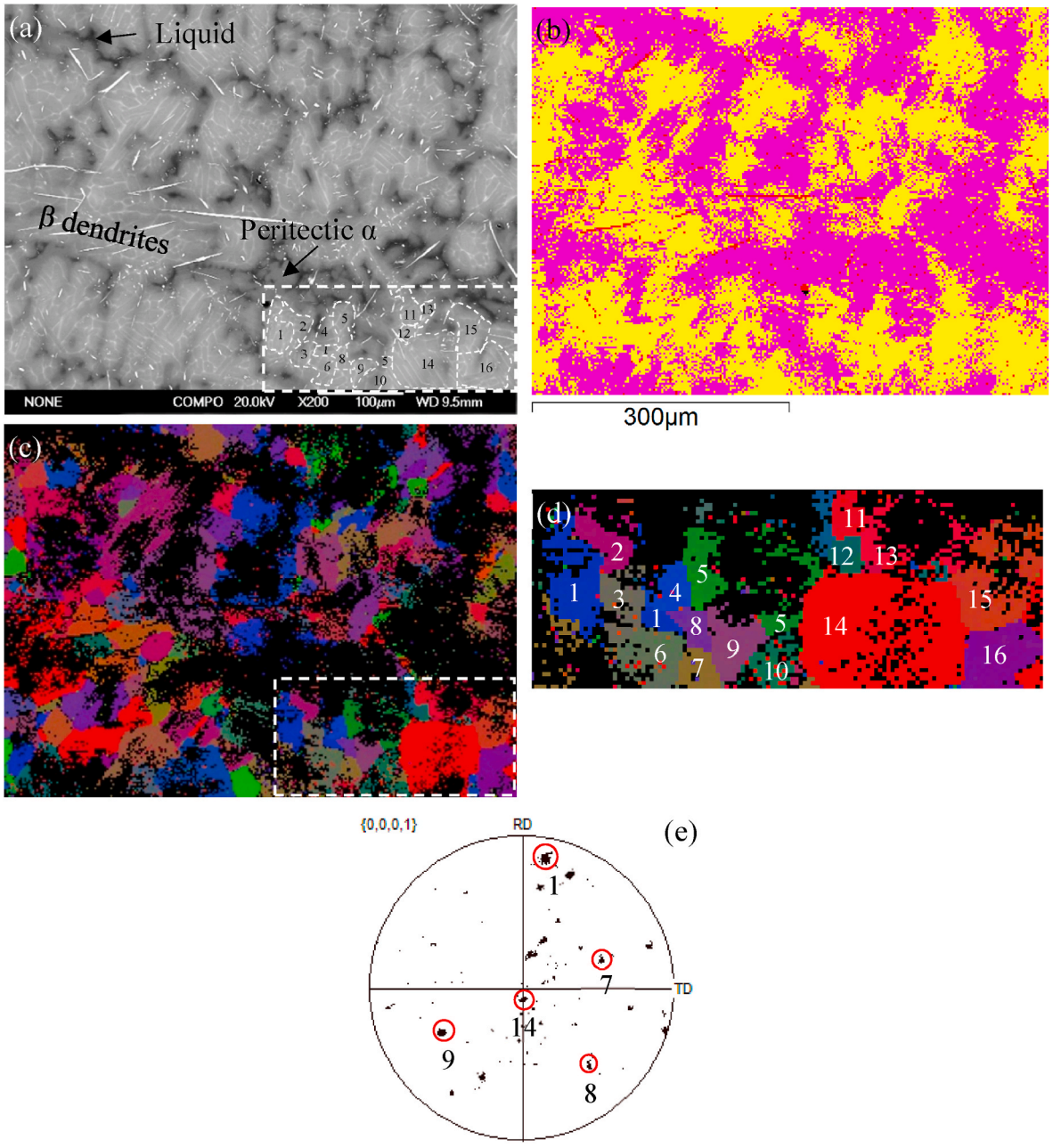

Fig. 5. Fine dendritic region in B4522Ta Bridgman sample showing (a) microstructure with original phase before quenching indicated, (b) phase map in which , and stand for α2, γ and TiB phases, respectively, (c) α2 phase normal direction orientation map, (d) enlarged α2 normal orientation map from the selected area in (c), (e) α (0001) pole figures of the selected grains.

Table 2
Angle between c-axes of the selected α_2 grains in fine dendritic region B4522Ta.

	α1	α7	α8	α9
α7	60.8			
α8	119.7	61.4		
α9	121.3	120.4	88.7	
α14	89.6	58.4	59.2	58.7

boundaries from the binary system. In this study, the orientation relationship between α_2 grains in the same dendrite was analysed in both the coarse and fine dendritic area of B4522Ta and B4522Hf. The purpose of this is to determine whether those α_2 grains have Burgers orientation relationship (OR) with the prior β dendrite. If the peritectic α grains are not Burgers α, it is possible that the peritectic α was inoculated by the boride precipitates at β/liquid interfaces during the peritectic reaction. The Burgers OR is that the hcp crystals are from the same bcc parent grain and obey

$$\{110\}_\beta // (0001)_\alpha;\ <111>_\beta // <2110>_\alpha \quad (3)$$

It can only be found out through the interrelationship between peritectic α grains because the β phase is already consumed and no longer exists. This technique involves a combination of EBSD mapping and mathematical calculation [8]. Essentially, a few α_2 grains adjacent to each other within the same dendrite were selected. The (0001) orientation of those α_2 grains were analysed using EBSD data and the signals from each α_2 grains yield a clear and definite spot in the pole figures. If they have Burgers OR, then the angle between the c-axes of any two α_2 grains can only be 0°, 60° or 90°. When two α variants precipitate from the same {110} in β, their (0001) are parallel and the angle between them is 0°. If two α variants precipitate from two {110} in β, whose zone axes are parallel to <100>, their (0001) are perpendicular to each other and the angle between them is 90°. When two α variants precipitate from two {110} in β, whose zone axes are parallel to <111>, the angle between their (0001) is 60°.

3.3.1. B4522Ta

An area in the coarse dendritic region was chosen for detailed analysis, with the BSE image and the EBSD phase map of this area are shown in Fig. 4 (a) and (b). The peritectic α grains have intermediate contrast between β dendrites and interdendritic liquid and are free from bright ridges. By comparing the BSE image in Fig. 4 (a) and the corresponding EBSD phase map in Fig. 4 (b), taken from the indicated region, the volume fraction difference between γ phase and interdendritic liquid can be observed. This suggests that a solid area existed here, likely being peritectic α prior to transformation into γ during quenching. The existence of peritectic α suggests that the L + β → α peritectic reaction should have occurred. The α_2 grains are randomly oriented as can be seen from the pole figure of the whole area in Fig. 4 (e). Some α_2 grains at the left part of the long dendrite at the middle of the image were selected for orientation analysis, as shown in Fig. 4 (d) with 18 α_2 grains numbered. A few α_2 grains e.g. grain No.7 surrounding the same interdendritic area have the same colour although they are located on different sides. They might be a single α_2 grain and connected to each other underneath the sample surface. All the numbered α_2 grains except for No. 8 have bright ridges inside. The right-side area of α grain No. 8 and 9 and area below grain No. 11 have no bright ridges at all although they were parts of the dendrite. It can be established that they were α whilst other parts of the dendrite were β before quenching according to the phase transformation history. Those α areas before quenching should be the peritectic α or at least related to the peritectic α having a high Al concentration which made it unstable during quenching and transformed into γ phase eventually. The (0001) pole figures derived from the selected region is shown in Fig. 4 (f). The angle between the c-axes of any two grains was measured from the pole figure. It is found that α_2 grains No. 6, 16 and 17 are Burgers α, as shown in Table 1, which are located away from the interdendritic γ grains, and are having the specific angle values, being either 60°or 90°. Therefore, peritectic α grain No.8, 9 and 11 could be non-Burgers variants. The breakdown of Burgers relationships indicates that those non-Burgers variants acquired orientation from something else rather than their parent β phase. The peritectic α is formed between

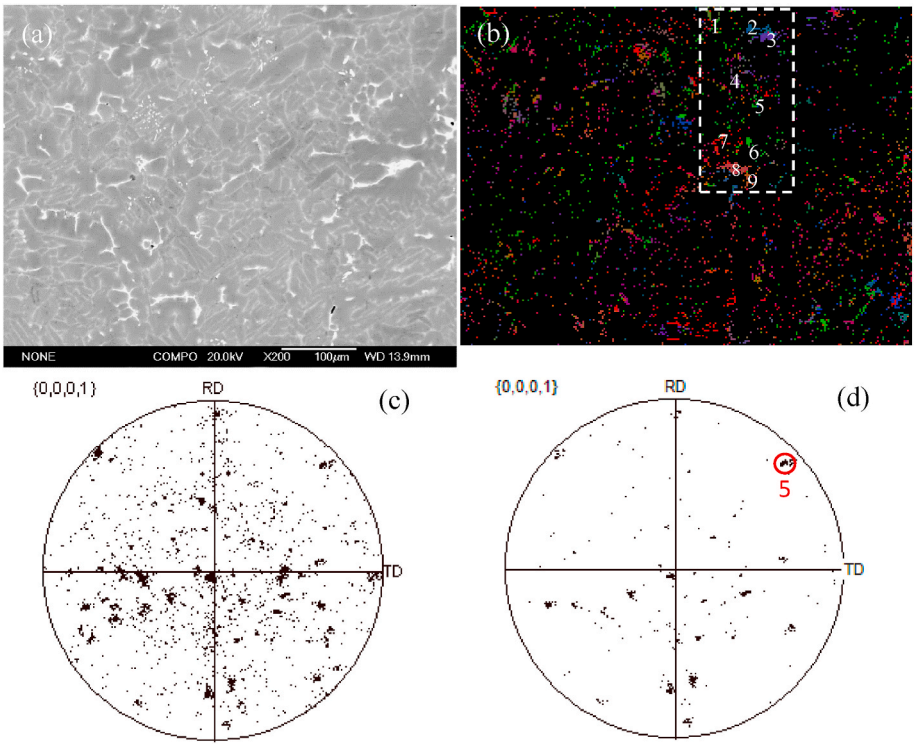

Fig. 6. Coarse dendritic region in B4522Hf Bridgman sample, showing (a)BSE image, (b) α_2 normal direction orientation map, (c) α (0001) pole figures from the whole area, (d) α (0001) pole figures from the selected area.

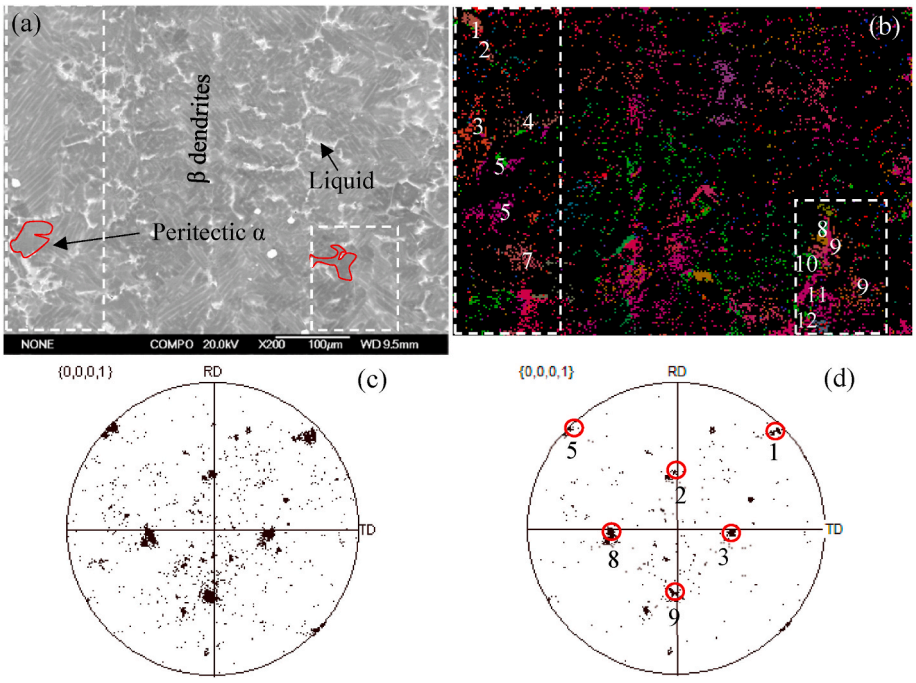

Fig. 7. Fine dendritic region in B4522Hf Bridgman sample, showing (a) microstructure with original phase before quenching indicated, (b) α_2 normal direction orientation map, (c) α (0001) pole figures from the whole area, (d) α (0001) pole figures from the selected area.

Table 3
Angle between c-axes of the selected α_2 grains in fine dendritic region in B4522Hf.

	α2	α3	α5	α8	α9
α3	57.6				
α5	59.4	120.7			
α8	58.9	91.2	60.6		
α9	90.8	60.5	120.8	59.7	
α10	61.6	62.7	121.2	119.6	120.4

the β dendrites and the liquid as thin layers, which acted as a seed for the β → α transformation passing its orientation to the α formed with β dendrites. In cases where boride precipitates are readily available at β/L interfaces, peritectic α can nucleate with an orientation defined by the boride rather than the β dendrites. These randomly orientated boride precipitates are essential for the formation of the non-Burgers α grains. The formation of borides must occur prior to the peritectic reaction otherwise the borides in the interdendritic region will not cause grain refinement.

Further Burgers variants are found in the fine dendritic area, with the BSE image and the EBSD phase map shown in Fig. 5 (a) and (b). The enlarged orientation map of this chosen area is shown in Fig. 5 (d) with 16 numbered á$_2$ grains. All the numbered á$_2$ grains have bright ridges inside. The (0001) pole figure derived from the selected region is shown in Fig. 5 (e). It is found that á$_2$ grains No. 1, 7, 8, 9 and 14 are one group of Burgers variants, while the others are not. Table 2 summarises the specific angle values of those α_2 grains indicating they are either 60° or 90° establishing that those α_2 grains are Burgers variants. The existence of more Burgers variants in the fine dendritic region indicates that the peritectic α acquired orientation from the β phase rather than boride precipitates. This is consistent with the microstructural observation, borides in the fine dendritic region are in the form of short rods and mainly located in the interdendritic region, which indicates that they must form after the peritectic reaction during quenching. Peritectic α was not able to be inoculated by the boride precipitates at the β/liquid interfaces and borides do not have time to grow at this stage. At the early stage of solidification, there are not many peritectic α grains as they can only form in the late stage of solidification when the Al is enriched in the interdendritic liquid regions.

3.3.2. B4522Hf

The BSE image of the coarse dendritic area is shown in Fig. 6 (a). In the BSE image, the strong contrast between β dendrite and interdendritic liquid can still be observed but in an opposite way compared with B4522Ta. Some α_2 grains at the top part of the long dendrite were selected for orientation analysis, as shown in Fig. 6 (b) with 9 numbered α_2 grains. All of those selected α_2 grains have bright ridges inside. Grain No.2 and No.3 are adjacent to the interdendritic liquid area and they should be peritectic α before quenching. The (0001) pole figures derived from the whole area and the selected region are shown in Fig. 6 (c) and (d), respectively. It is found that there is only grain No. 5 belongs to Burgers family, while grain No.2, 3 and the others are not. The loss of Burgers OR was attributed to the process that the peritectic α was inoculated by the boride precipitates at β/liquid interfaces during the peritectic reaction.

The BSE image of the fine dendritic area is shown in Fig. 7 (a) where the volume fraction of peritectic α grains are decreased and less apparent at a late stage of solidification. The α_2 normal direction orientation map is shown in Fig. 7 (b). Two particular areas, as marked with white dashed rectangles, were selected for further OR analysis. Twelve of the α_2 grains were selected, with all having bright ridges inside. However, grain No. 5, 8, 9 and 10 which are adjacent to the interdendritic area, plus the area below grain No.5 and the area on the left side of grain No.8 and 10 have no bright ridges even though they were parts of the dendrite. The (0001) pole figures derived from the whole area and the selected regions are shown in Fig. 7 (c) and (d), respectively. It is found that six pairs which labelled as grain No.2, 3, 5, 8, 9 and 10 are one group of Burgers variants, and the others are not. Table 3 summarises the specific angle values of those α_2 grains.

It is worth noting that the difference in vol. % of α_2 grains on the EBSD phase map between B4522Ta and B4522Hf is striking. The vol. % of α_2 grains can be as low as 7.3% in B4522Hf, whereas in B4522Ta the lowest vol. % of α_2 grains is found to be 31.1%. Upon quenching, there is

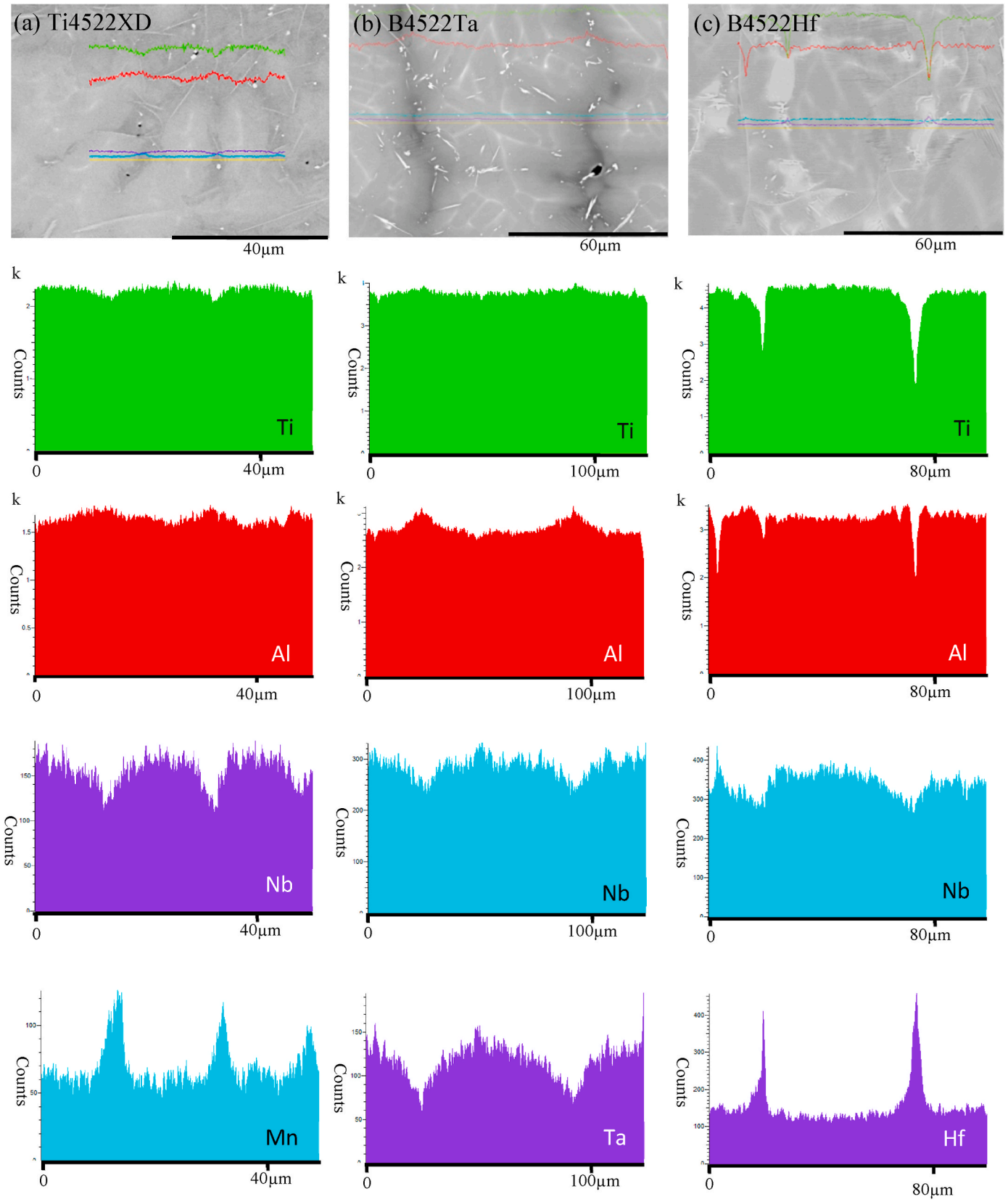

Fig. 8. Microstructure of the alloys (a) Ti4522XD, (b) B4522Ta and (c) B4522Hf and corresponding quantitative concentration line profiles obtained by EDS analysis. The concentration profiles show the distribution of alloying elements along the lines marked on the micrographs.

still a large volume of α_2 grains retained in B4522Ta, whereas the very small volume of α_2 grains was retained in B4522Hf as they were fully transformed into γ plates. Small α lamellae formed, which cannot be distinguished by the smallest EBSD pixel size (1.375 μm^2) available, as such it is clear that Ta is more effective in stabilizing α than Hf.

3.4. Microsegregation

EDS analysis was performed in the solidification zone of B4522Ta, B4522Hf and used the Ti4522XD base alloy as a reference. The microstructure of the alloys along with quantitative composition line profiles of Ti4522XD, B4522Ta and B4522Hf are shown in Fig. 8. Quantitative EDS analysis of Ti4522XD revealed that the dendrite cores were rich in Nb, Ti and depleted in Al whereas the interdendritic regions were rich in Al and Mn, depleted in Nb and Ti, clearly indicating that the peritectic α phase has formed in these regions. The above observation is consistent with the results from Imayev et al. [17]. The line profile of B4522Ta indicates that the dendrite cores were rich in Nb and Ta and depleted in Al whereas the interdendritic regions were rich in Al, poor in Nb and Ta, with little microsegregation of Ti in this alloy. The β stabilizing elements here are Nb and Ta which were expelled from the newly formed α to the remaining β, therefore, the dendritic region is enriched with Nb and Ta. On the contrary, the concentration line profiles of B4522Hf show that dendrite cores were rich in Ti, Al and Nb and depleted in Hf whereas the interdendritic regions were rich in Hf but depleted of Ti, Al and Nb. This sudden drop in Al in the spectrum is caused by precipitation of oxides (revealed as white particles). The Al concentration increased/decreased before reaching/after leaving the particles, which indicates that alloys with Hf addition show lower oxidation resistance than those containing Ta. The above observations corroborate that the addition of β stabilizing elements, Nb and Ta, are beneficial to prevent peritectic growth and thus maintain the refining capability of boron, while Hf is not a β stabilizing element and is shown not to prevent peritectic growth [5].

4. Conclusions

The following can be concluded regarding the solidification behaviour in Bridgman samples:

- Ta, Hf are shown to have different effects on boride precipitation temperature (relative temperature in L + S region). In B4522Ta, the start of primary boride precipitation was found slightly later than the leading β phase, whereas, in B4522Hf, the boride formation occurred well after the β dendrites were formed, likely at a stage when the β dendrite growth was almost at its end.
- The orientation relationship analysis of peritectic α grains in B4522Ta and B4522Hf reveal the loss of Burgers OR. This is attributed to the process whereby the peritectic α was inoculated by the boride precipitates at β/liquid interfaces during the peritectic reaction. The effect of Ta and Hf on the peritectic reaction was similar.
- The microsegregation data collected indicates that the interdendritic regions were lean Ta in B4522Ta, whereas, the interdendritic regions were rich in Hf in B4522Hf. The addition of β stabilizing elements e.g. Nb and Ta are beneficial to prevent peritectic growth and thus maintain the refining capability of boron. Hf is not a β stabilizing element and is not beneficial to prevent peritectic growth.

CRediT authorship contribution statement

Jing Li: Data curation, Investigation, Writing - original draft, Writing - review & editing. **Spencer Jeffs:** Writing - review & editing, Supervision. **Mark Whittaker:** Writing - review & editing, Supervision. **Nigel Martin:** Validation, Funding acquisition.

Declaration of competing interest

The authors declare that they have no known competing financial interests or personal relationships that could have appeared to influence the work reported in this paper.

Acknowledgements

The research was funded by the EPSRC Rolls-Royce Strategic Partnership in Structural Metallic Systems for Gas Turbines (grants EP/H500383/1 and EP/H022309/1). The provision of materials and technical support from Rolls-Royce plc. is gratefully acknowledged. EBSD work was performed at the University of Birmingham. The author would like to thank Dr Dawei Hu for his supervision on this study.

References

[1] Y.-W. Kim, S.-L. Kim, Advances in gammalloy materials–processes–application technology: successes, dilemmas, and future, JOM 70 (4) (2018) 553–560.
[2] D. Hu, Role of boron in TiAl alloy development: a review, Rare Met. 35 (1) (2016) 1–14.
[3] Q. Wang, R. Chen, X. Gong, J. Guo, Y. Su, H. Ding, H. Fu, Microstructure, mechanical properties, and crack propagation behavior in high-Nb TiAl alloys by directional solidification, Metall. Mater. Trans.: Physical Metallurgy and Materials Science 49 (10) (2018) 4555–4564.
[4] J. Schuster, M. Palm, Reassessment of the binary aluminum–titanium phase diagram, J. Phase Equilibria Diffus. 27 (2006) 255–277.
[5] U. Hecht, V. Witusiewicz, A. Drevermann, J. Zollinger, Grain refinement by low boron additions in niobium-rich TiAl-based alloys, Intermetallics 16 (8) (2008) 969–978.
[6] K. Kamyshnykova, J. Lapin, Grain refinement of cast peritectic TiAl-based alloy by solid-state phase transformations, Kovove Mater. 56 (5) (2018) 277–287.
[7] D. Hu, A quarter century journey of boron as a grain refiner in TiAl alloys, in: TMS Annual Meeting, 2014.
[8] D. Hu, C. Yang, A. Huang, M. Dixon, U. Hecht, Solidification and grain refinement in Ti45Al2Mn2Nb1B, Intermetallics 22 (2012) 68–76.
[9] T.T. Cheng, The mechanism of grain refinement in TiAl alloys by boron addition — an alternative hypothesis, Intermetallics 8 (1) (2000) 29–37.
[10] J. Li, S. Jeffs, M. Whittaker, N. Martin, Boride formation behaviour and their effect on tensile ductility in cast TiAl-based alloys, Mater. Des. 195 (2020) 109064.
[11] B.G. Liu, L.H. Liu, W.D. Xing, R.C. Liu, R. Yang, P.A. Withey, J. Zhu, R. Yu, Structural stability and the alloying effect of TiB polymorphs in TiAl alloys, Intermetallics 90 (2017) 97–102.
[12] B. Liu, J. Li, D. Hu, Solidification and grain refinement in Ti(48–50)Al2Mn2Nb1B alloys, Intermetallics 101 (2018) 99–107.
[13] J. Lapin, Z. Gabalcová, Solidification behaviour of TiAl-based alloys studied by directional solidification technique, Intermetallics 19 (6) (2011) 797–804.
[14] X. Wu, Review of alloy and process development of TiAl alloys, Intermetallics 14 (10) (2006) 1114–1122.
[15] H. Fang, R. Chen, X. Chen, Y. Yang, Y. Su, H. Ding, J. Guo, Effect of Ta element on microstructure formation and mechanical properties of high-Nb TiAl alloys, Intermetallics 104 (2019) 43–51.
[16] L.-H. Ye, H. Wang, G. Zhou, Q.-M. Hu, R. Yang, Phase stability of TiAl-X (X=V, Nb, Ta, Cr, Mo, W, and Mn) alloys, J. Alloys Compd. 819 (2020) 153291.
[17] R.M. Imayev, V.M. Imayev, M. Oehring, F. Appel, Alloy design concepts for refined gamma titanium aluminide based alloys, Intermetallics 15 (4) (2007) 451–460.